Theor Chem Acc (2001) 105:354–359
DOI 10.1007/s002140000240

Theoretical
Chemistry Accounts

Regular article

Theoretical study of group 11 metal–silonyl complexes: *M*–SiO and *M*–$(SiO)_2$ (*M* = Cu, Ag, or Au)

D. Mandelbaum, M. E. Alikhani

LADIR/Spectrochimie Moléculaire (UMR 7075), Université P. et M. Curie, Boîte 49, bâtiment F74, 4 Place Jussieu Paris Cedex 05, France

Received: 6 July 2000 / Accepted: 11 October 2000 / Published online: 19 January 2001

Abstract. The spectroscopic properties of *M*–SiO and *M*–$(SiO)_2$ (1–1 and 1–2 complexes with *M* = Cu, Ag, or Au) have been theoretically studied. It has been shown that both *M*–SiO and *M*–$(SiO)_2$ compounds in their ground state are bent with a metal–Si bonded structure. The calculated *M*(*ns*) spin density agrees well with the electron spin resonance experimental data. From a topological analysis, it has been shown that a rather large charge transfer occurs from the metal towards the SiO moiety, and that the *M*–Si bond energy correlates with the electron density located at the *M*–Si bond path (bond critical point).

Key words: Bond critical point – Metal–silonyl complexes – Bader analysis – Pseudopotential – Spin density

1 Introduction

The interactions involving transition-metal atoms play an essential role in surface and material science. It is of the utmost important to be able to perform an accurate theoretical description of such a system. It is now well established that the quantum chemical calculation of transition-metal compounds requires the explicit treatment of electron correlation and relativistic effects [1, 2]. In particular, the relativistic effects must be taken into account when the chemical compound involves the third transition-metal atoms [2].

Density functional theory (DFT) including the exchange–correlation functional seems an adequate approach to study such a system [3]. In particular, the hybrid approach proposed by Becke [4] manages the advantages of Hartree–Fock and DFT models with an improved overall accuracy [5, 6]. A number of theoretical studies have shown that (B3LYP) variant is particularly effective in the description of the physicochemical properties of the binary complexes [7–9].

Among small transition-metal complexes, metal–monocarbonyls, *M*(CO), have been studied extensively both experimentally [10–22] and theoretically [2, 3, 7–9, 23–32]; whereas the corresponding *M*–(SiO) is not yet sufficiently investigated [33–39]. The IR and electron spin resonance (ESR) properties of *M*:CO (*M* = Cu, Ag, or Au) have been measured in several experimental works [12–14, 19, 20, 21, 36]. These complexes have also been studied using several theoretical methods [8, 9, 28, 30, 31]. From both experimental and theoretical points of view, it has been shown that the Ag:CO complex would be actually a weak van der Waals complex (bound by only 40–50 cm^{-1}), dissociating into Ag and CO [2, 20, 28]. From ESR experiments, the Cu–Co and Au–CO complexes were found to be linear ($^2\Sigma$ electronic state) [36], whereas the theoretical investigations proposed a bent structure [2, 8, 31]. Using DFT calculations Barone (5) showed that the linear Cu–CO corresponds to a transition state. In recent experimental work, the three fundamental vibrational modes were identified with the help of isotopic effects and it has been evidenced that the Cu–CO complex actually has a bent geometry [11, 40]. It is worthy noting that the ESR and IR experiments are required to predict the structure of the metal–ligand compounds. Furthermore, in the case of Ag–SiO it has been shown that the vibrational data obtained from IR experiments [33] and the density of spin located on the Ag atom measured from ESR [34, 36] are only theoretically well reproduced for a bent structure [39], although the ESR experiment suggested only a linear geometry [36]. In the case of the Cu(SiO) and Au(SiO) complexes, a linear structure for Cu(SiO) and a bent structure for Au(SiO) were suggested from the ESR spectra. To our knowledge, there are no IR results for these systems.

Therefore, we thought it interesting to understand if the *M*(SiO) and *M*$(SiO)_2$ (*M* = Cu, Ag, or Au) are bent or linear, Si-bonded or O-bonded structures. In order to calculate the structural, energetic, and vibrational

Correspondence to: M. E. Alikhani
e-mail: ea@spmol.jussieu.fr

Contribution to the Proceedings of the 2000 Symposium on Chemical Bonding: State of the Art in Conceptual Quantum Chemistry

properties, these compounds were investigated using the DFT/hybrid method. Furthermore, the nature of *M*–Si bonding was studied using the topological theories of atoms in molecules (AIM) [41] and of the electron localization function (ELF) [42].

2 Results and discussion

All the calculations were performed with the Gaussian 94/DFT quantum chemical package [43]. The DFT calculations were carried out with B3LYP [44]. We used the 19-valence electron of the Stuttgart pseudopotential for the group 11 metals (relativistic for Cu [45] and pseudorelativistic for Ag and Au [46]) and the 6-311 + G(2d) extended basis set of Krishnan et al., Clark et al., and Frisch et al. [47–49] for the other atoms. The topological properties were investigated using the Top-Mod package [50] and the program EXTREME (part of the AIMPAC suite of programs) developed by Konig et al. [51].

2.1 Structural and vibrational analysis

2.1.1 1–1 complexes: *M*(SiO)

Five geometries were studied for all the compounds (Fig. 1) at the DFT/B3LYP level of theory. The linear and bent *M*–OSi structures (Fig. 1a, b) are found to be unbound in all of the cases. The cyclic geometry (Fig. 1c) is calculated to be bound only for Cu(SiO). For two other complexes, Ag(SiO) and Au(SiO), the triangular structure collapses to a bent metal–Si bonded structure upon optimization. Concerning the metal–Si bonded structures (Fig. 1d, e), it has been shown that the bent structure is more stable than the linear one. A vibrational analysis of the linear *M*–SiO compounds (in the $^2\Sigma$ electronic state) indicates that this geometry actually corresponds to a transition state (two imaginary frequencies with π symmetry). The barrier height for the inversion isomerization of Cu–(SiO) was found to be 9.3 kcal/mol. In the case of Cu(SiO), the bent metal–Si bonded structure is slightly more stable than the cyclic one, indicating that the cyclic complex is a metastable structure. Furthermore, the barrier height in going from the bent end-bonded complex to the side-bonded structure is very small (0.6 kcal/mol), allowing directly the formation of the bent structure even at low temperatures. These results allow one to consider the bent *M*–SiO structure as the ground electronic state (^{2}A′). Therefore, in the following we study only the bent *M*–SiO geometry. The spectroscopic properties of the 1–1 complexes are reported in Table 1. In all the 1–1 complexes, the Si–O bond length is slightly longer than that of free SiO. The Si–O lengthening decreases from Cu–SiO to Au–SiO. The *M*SiO bond angle was calculated to be around 120°. Since this value is much smaller than 180°, we can conclude that the bent structure can not be due to a Jahn–Teller effect. For all the compounds, the Si–O bond length remains less than 1.550 Å, which is in the range of Si=O double bonds [52]. The *M*–Si bond length varies as Cu–SiO < Au–SiO < Ag–SiO. There is not a linear relation between the binding energies and the *M*–Si bond length. We should note that the binding energy actually depends on two contributions: the bond energy between metal and Si atoms and that of silonyl part. These contributions make up for each other. As expected, the Si–O bond lengthening correlates with the SiO frequency shift and the Si–O force constant, but it is not related to the binding energy. The enhancement of the *M*–SiO dipole moment with respect to free SiO is in line with the IR intensity of SiO vibrational frequency. The experimental observation of the Si*M* stretch and *M*SiO bending modes seems very difficult because of their weak IR intensities. Finally, as shown in Table 1 the calculated *s* character of spin density of the unpaired electron located on the metal atom agrees well with the experimental result [36].

2.1.2 1–2 complexes: $M(SiO)_2$

The spectroscopic parameters of $M(SiO)_2$ calculated from DFT techniques are reported in Table 2. The

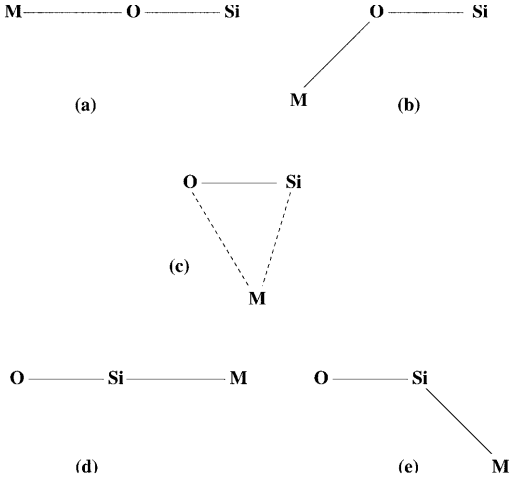

Fig. 1. Possible geometries for the 1–1 complex *M*(SiO)

Table 1. Structural and vibrational parameters of bent *M*–SiO in the ^{2}A′ state

Parameters	Cu–SiO	Ag–SiO	Au–SiO	SiO
r_1 (Å)	1.528	1.526	1.524	1.514
r_2	2.328	2.558	2.360	
∠a (deg)	120.0	114.5	127.8	
D_e (kcal/mol)[a]	13.2	8.1	19.2	
μ (D)	4.24	4.08	3.72	3.23
$\rho_s(M)$ (%)	61	74	56	
$\rho_s(M)$[b]	71	74	54	
SiO stretch (cm^{-1})[c]	1187[133]	1192[125]	1198[104]	1246[56]
Experiment		1163[d]		1242[e]
Si*M* stretch	229[3]	182[6]	268[7]	
*M*SiO bend	108[3]	93[5]	136[3]	
f_{SiO} (mdyn/Å)	8.5	8.6	8.6	9.3

[a] $D_e = (E_M + E_{SiO}) - E_{M-SiO}$
[b] Experimental values deduced from Ref. [36]
[c] The calculated IR intensities (km/mol) are reported in brackets
[d] Ref. [33]
[e] Ref. [57]

Table 2. Structural and vibrational parameters of bent M–$(SiO)_2$ in the $^2A_1$ state

Parameters	Cu–$(SiO)_2$	Ag–$(SiO)_2$	Au–$(SiO)_2$
r_1 (Å)	1.522	1.522	1.520
r_2	2.371	2.576	2.452
$\angle a$ (deg)	129.1	123.9	131.2
$\angle b$	168.1	168.7	165.2
D_e[a]	9.9	7.2	12.8
$\rho_s(M)$ (%)	38	44 (50[b])	30
μ (D)	5.84	5.84	5.41
SiO symmetric stretch (cm^{-1})[c]	1218[48]	1218[57]	1222[46]
SiM symmetric stretch	189[2]	161[1]	196[1]
MSiO symmetric bend	130[1]	104[0.5]	150[3]
SiMSi bend	26[4]	24[2]	27[2]
MSiO asymmetric bend (O.P.)	23[0]	16[0]	34[0]
MSiO symmetric bend (O.P.)	41[9]	34[11]	50[18]
SiO asymmetric stretch	1203[437]	1205[412]	1209[335]
SiM asymmetric stretch	231[0.2]	183[1]	232[3]
MSiO asymmetric bend	103[0.1]	94[0.3]	109[0.2]
f_{SiO} (mdyn/Å)	8.8	8.8	8.9

[a] $D_e = (E_{M-SiO} + E_{SiO}) - E_{M-(SiO)_2}$
[b] Experimental value deduced from Ref [36]
[c] The calculated IR intensities (km/mol) are reported in brackets

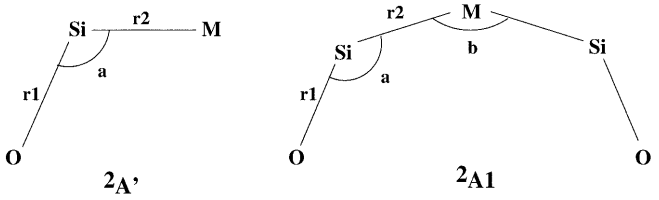

Fig. 2. The most stable structures of the M(SiO) and $M(SiO)_2$ compounds

geometrical parameters are displayed in Fig. 2. To our knowledge, there is no IR experimental data on the 1–2 complexes. Only the spin density of the unpaired electron located on Ag in $Ag(SiO)_2$ is measured from ESR experiments [34, 36].

We have found that the M–$(SiO)_2$ complex is bound with respect to the M + 2SiO and to the M–SiO + SiO subunits. All of our computed D_e values (Table 2) are for the process $M\text{–}(SiO)_2 \rightarrow M + M$SiO. The zero-point correction for such a process is expected to be very small, since the decrease in the M–Si vibrational frequency cancels the increase in the SiO vibrational frequency. For all three complexes the binding energy per silonyl is found to be slightly lower for the disilonyl complexes than for the monosilonyl complexes. For both the monosilonyl and disilonyl complexes, Au is found to be most strongly bound, Cu the next most strongly bound, and Ag the most weakly bound. This finding is in line with all experimental and theoretical data on the thermodynamic stability of the group 11 carbonyls (Au ≈ Cu ≫ Ag) [53]. Enhanced metal–ligand stability in gold compounds is often explained in terms of relativistic effects [1]. The geometrical variations in the M–$(SiO)_2$ complex follow the same trend as those in the M–SiO compound. The Si–O bond length in the M–$(SiO)_2$ system is found to be slightly smaller than that in the M–SiO one, while the lengthening of the M–Si bond is more pronounced in going from M–SiO to M–$(SiO)_2$. The MSiO bond angle in the 1–2 complex is slightly larger than that in the 1–1 complex. It is in line with the inversion barrier height which was found to be 7.5 kcal/mol, for the bent $Cu(SiO)_2 \rightarrow$ linear $Cu(SiO)_2$ transformation. The SiMSi bond angle was calculated to be around 168°, consistent with the barrier height for going from the bent SiMSi to the linear SiMSi (less than 1 kcal/mol).

The predicted frequency shift of the SiO stretch for the M–$(SiO)_2$ complex is sufficiently different from that for M–SiO, allowing this band to be observed experimentally. The other vibrational frequencies are found to be very low and relatively weak, so their experimental observation would be difficult.

The dipole moment is even enhanced in going from M–SiO to M–$(SiO)_2$, leading to the increase in the IR intensity of the SiO asymmetric stretching mode.

Finally, the predicted s spin density located at the metal upon complexation allows us to hope that it can be observed experimentally using the ESR technique.

2.1.3 Bonding considerations

As in the case of the $M(CO)_x$ systems, the bonding in the $M(SiO)_x$ complexes is dative in character and so is characterized by a simple donor–acceptor mechanism. The strength of the M–SiO bond is determined by a balance between π back donation from the metal to the SiO π^* orbital and the σ donation from the Si lone pair to the vacant orbital of the metal. The latter interaction (σ donation) is essentially repulsive. To reduce this repulsion, several mechanisms were suggested: $4s$ to $3d$ promotion and $4s - 3d_\sigma$ hybridization [23]. The first mechanism to reduce the σ repulsion takes place when the promotion energy required for the electronic rearrangement on the metal atom is low as in the case of the NiCO compound for example. The $4s - 3d_\sigma$ hybridization generally leads to a linear structure of the metal–ligand complex (NiCO, for example) [29]. For the Cu–CO complex, the $4s - 3d_\sigma$ hybridization does not take place, since Cu has a filled d shell in its ground state. This is essentially why CuCO is only bound in a bent structure [29]. We can similarly explain the bent bound structure for the complexes studied in this work.

Furthermore, to obtain a deeper understanding of the bonding between group 11 metals and SiO, we studied the systems using a topological analysis of a localization function by means of the ELF [42] and of the theory of AIM [41]. We should note that, in principle, the topological analysis of the ELF is restricted to all-electron wavefunctions. Recently, Joubert et al. [54] showed that with small core pseudopotentials the external part of the core gives rise to a well-defined basin which shares separatrices with the surrounding valence basins; therefore, the analysis can be carried out safely. Here, the topological data obtained by a combined ELF/AIM approach was done with a small core pseudopotential.

2.1.3.1 Laplacian of the charge density analysis. The calculated topological properties at the bond critical points are listed in Table 3. According to the topological

theory of AIM [41] the positive values of the electron density Laplacian at the bond critical point (where $\nabla\rho = 0$) are associated with closed-shell interactions (ionic bonds, hydrogen bonds, and van der Waals molecules), while $\nabla^2\rho < 0$ indicates shared interactions (covalent bonds). Another criterion, proposed by Cremer and kraka [55], states that the local energy density, H, at the bond critical point should be positive for ionic bonds and negative for partly covalent bonds. The results reported in Table 3 show that, following this criterion, the Si–O bond should be considered as a shared interaction for all compounds, because of the negative energy density at the Si–O bond critical point. The large positive values of $\nabla^2\rho$ at the Si–O bond critical point indicate a polar displacement toward oxygen. However, the bonding between the metal atom and silicon within both the M–SiO and M–$(SiO)_2$ complexes presents a very weak covalent character because of the very small negative value for the energy density at the M–Si bond critical point.

It is very interesting to note that the binding energy between the metal and each ligand ($M + SiO$ and $M + MSiO$) nicely correlates with the electron density calculated at the M–Si bond critical point. For all of the compounds studied in this work, the correlation coefficient calculated for the binding energy per SiO ligand as function of $\rho(M\text{–Si})$ is very close to 1 (0.96).

2.1.3.2 Topological analysis of the ELF function. In the ELF approach, the molecular space is partitioned into basins of attractors which have a clear chemical signification. These basins are either core basins surrounding nuclei or valence basins. The valence basins are characterized by their synaptic order, which is the number of core basins with which they share a common boundary. Accordingly, monosynaptic basins correspond to lone-pair regions, labeled as $V(X)$, where X denotes an atom label, whereas disynaptic ones correspond to bonding regions, labeled as $V(X, Y)$, where X and Y denote atom labels. A complete and detailed description of this nomenclature can be found in Ref. [50].

The topological data obtained from the Top-Mod package are reported in Table 4. The bonding between metal and ligand takes place through a charge transfer from the metal to the lone-pair basin of the Si atom. As shown in Figs. 3 and 4, the $V(M, \mathrm{Si})$ basin is mostly located on the Si atom. The metal charge participation in the $V(M, \mathrm{Si})$ basin is given by $V(M, \mathrm{Si})/M$. It indicates the net charge of the metal atom in the complex. It has been found that the charge transfer from Cu is much larger than that from Ag and Au; however, this bond formation could be essentially considered as a dative bond. In addition, there is charge reorganization between the V(Si,O) and V(O) basins upon complexation. In other words, the V(O) population increases when the V(Si,O) population decreases. This effect explains why the polarity of the Si–O moiety increases, which is justified by the augmentation of the dipole moment of the complex. By inspecting Table 4, one can understand why the linear M–(SiO) structure does not correspond to the ground electronic structure. In the linear CuSiO compound the charge transfer from metal to ligand and the charge reorganization between the shared V(Si,O) basin and the nonbonding V(O) one are smaller than in the bent CuSiO complex. These considerations are in line with the AIM's atomic charge of the metal atom calculated from the Top-Mod programs [$Q(M)$ in Table 4]. One can check, for example, the net charge of the Cu atom [$Q(M)$-19] in the linear CuSiO complex is -0.08e while it is positive (0.07e) for the bent CuSiO compound. Therefore, the stability of the group 11 metal–silonyl complexes arises mostly from two electronic charge transfers: from the outer-core population of the metal atom to the lone-pair basin of Si and the other from the disynaptic V(Si,O) basin to the lone-pair basin of the O atom.

Concerning the bent geometry of the complexes studied, we can consider the MSiO or the SiMSi moieties as the AX_2E_2 species in the valence-shell electron pair repulsion theory [56]. It is interesting to note that in the MSiO and $M(SiO)_2$ complexes, the MSiO bond angle varies as the V(O) population varies. The repulsion

Table 3. Bond critical point (*bcp*) data of M–SiO and M–$(SiO)_2$ from the atoms in molecules method. ρ and H represent the electron density and energy density at the bcp

Compounds	Si–O bcp			M–Si bcp		
	ρ	$\nabla^2\rho$	H	ρ	$\nabla^2\rho$	H
SiO	0.193	1.46	−0.099			
Cu–SiO	0.187	1.36	−0.096	0.062	0.03	−0.020
Ag–SiO	0.188	1.38	−0.096	0.052	0.03	−0.015
Au–SiO	0.188	1.38	−0.097	0.079	−0.03	−0.038
Cu–$(SiO)_2$	0.189	1.40	−0.098	0.058	0.05	−0.018
Ag–$(SiO)_2$	0.190	1.41	−0.098	0.051	0.04	−0.014
Au–$(SiO)_2$	0.190	1.41	−0.098	0.070	0.01	−0.026

Table 4. Basin populations of M–SiO and M–$(SiO)_2$ calculated from electron localization function analysis. $V(X, Y)$ = the shared basin between X and Y; V(O) = the valence nonbonding of oxygen; $C(M)$ = the outer core basin of the metal; $V(M, \mathrm{Si})/M$ = the population of $V(M, \mathrm{Si})$ with the M part; and σ = the standard deviation of the corresponding basin

Compounds	$V(M, \mathrm{Si})/M$	σ	$V(\mathrm{Si}, \mathrm{O})$	σ	V(O)	$C(M)$	σ	$Q(M)$[a]
SiO	2.37/0.00	0.88	3.37	1.23	4.08			
CuSiO (bent)	4.00/1.63	1.90	2.89	1.39	4.51	17.37	1.09	18.93
CuSiO (linear)	3.20/0.83	1.31	3.07	1.22	4.38	18.17	1.07	19.08
AgSiO (bent)	2.80/0.41	1.86	2.93	1.07	4.46	18.57	0.78	18.92
AuSiO (bent)	2.79/0.44	1.19	2.70	1.60	4.71	18.56	0.93	18.60
Cu$(SiO)_2$ (bent)	3.17/0.80	1.21	2.90	1.20	4.53	17.32	1.09	19.0
Ag$(SiO)_2$ (bent)	2.75/0.38	1.10	2.88	1.21	4.51	18.23	0.96	19.0
Au$(SiO)_2$ (bent)	2.75/0.38	1.15	2.73	1.18	4.72	18.21	1.09	19.0

[a] $Q(M)$ is the outer-core population on the metal atom after atoms in molecules analysis

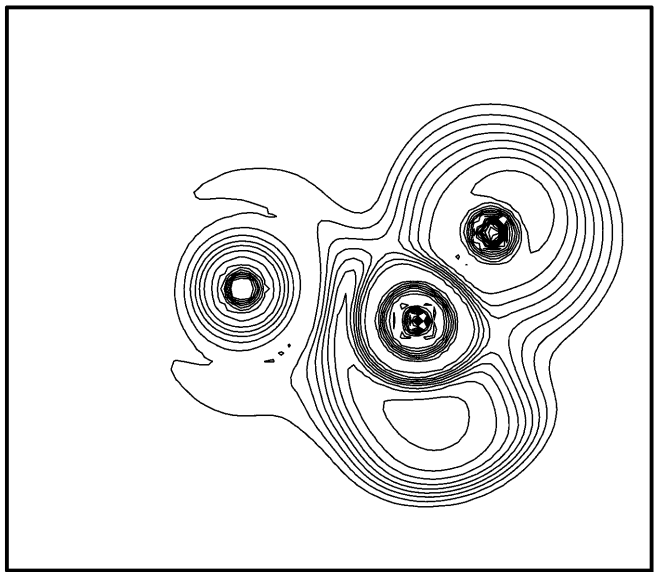

Fig. 3. Contour maps of the electron localization function (*ELF*) for the bent CuSiO complex

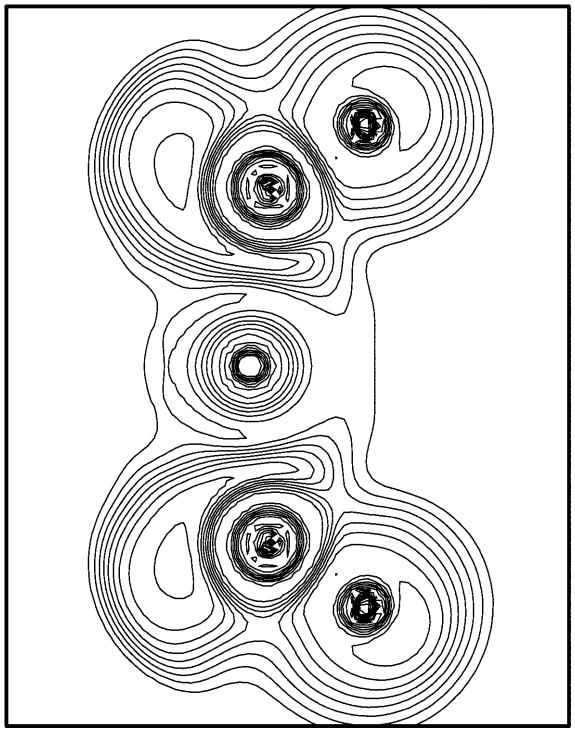

Fig. 4. Contour maps of the ELF for the bent $Cu(SiO)_2$ complex

between the outer-core basin of the metal and the lone-pair basin of O determines the *M*SiO bond angle value. One can verify this feature for all the compounds as follows: ∠AgSiO < ∠CuSiO < ∠AuSiO. We should note that in going from the 1–1 complex to the 1–2 complex the additional repulsion between ligand–ligand tends to increase the *M*SiO bond angle. Similarly, the Si*M*Si bent geometry in the $M(SiO)_2$ systems could be understood as a large ligand–ligand repulsion.

3 Concluding remarks

It has been shown that both the 1–1 and 1–2 complexes studied here are found to be bound in a bent structure. The available experimental data are very well reproduced from DFT calculations.

A combined ELF/AIM topological analysis has allowed the stability and structural properties to be understood. First, it seems reasonable to consider the electron density located at the metal–ligand bond critical point as a measure of the bond strength. Secondly, the bonding between group 11 metal and SiO should be mostly considered as a dative bond with a rather large charge transfer from the metal atom to the ligand. Finally, the *M*SiO and Si*M*Si bond angles in the complexes should be regarded as a result of the repulsion between the outer core of the metal and the lone-pair of the O atom and the ligand–ligand repulsion.

References

1. Pyykö P (1988) Chem Rev 88: 563
2. Schwerdtfeger P, Bowmaker GA (1994) J Chem Phys 100: 4487
3. Chung S-C, Krüger S, Pacchioni G, Rösch N (1995) J Chem Phys 102: 3695
4. Becke AD (1993) J Chem Phys 98: 5648
5. Becke AD (1993) J Chem Phys 98: 1372
6. Bauschlicher CW Jr, Partridge H (1995) J Chem Phys 103: 1788
7. Barone V (1995) Chem Phys Lett 233: 129
8. Barone V (1995) J Phys Chem 99: 11659
9. Adamo C, Lelj F (1995) J Chem Phys 103: 10605
10. Joly HA, Manceron L (1998) Chem Phys 226: 61
11. Tremblay B, Manceron L (1999) Chem Phys 242: 235
12. Chenier JHB, Hampson CA, Howard JA, Mile B (1988) J Phys Chem 92: 2745
13. Chenier JHB, Hampson CA, Howard JA, Mile B (1989) J Phys Chem 93: 114
14. Chenier JHB, Howard JA, Joly HA, Tomieto M (1989) Can J Chem 67: 655
15. Huber H, Kündig EP, Moskovits M, Ozin GA (1975) J Am Chem Soc 97: 2097
16. Hanlan L, Huber H, Ozin GA (1976) Inorg Chem 15: 2592
17. McIntosh D, Ozin GA (1976) J Am Chem Soc 98: 3167
18. McIntosh D, Ozin GA (1977) Inorg Chem 16: 51
19. Kasai PH, Jones PM (1985) J Am Chem Soc 107: 813
20. Kasai PH, Jones PM (1985) J Phys Chem 89: 1147
21. Kasai PH, Jones PM (1985) J Am Chem Soc 107: 6385
22. Van Zee RJ, Bach SBH, Weltner W Jr (1986) J Phys Chem 90: 583
23. Barnes LA, Bauschlicher CW Jr (1989) J Chem Phys 91: 314
24. Smith GW, Carter EA (1991) J Phys Chem 95: 2327
25. Mattar SM, Hamilton W (1991) J Mol Struct (THEOCHEM) 226: 147
26. Jeung G (1992) J Am Chem Soc 114: 3211
27. Sodupe M, Bauschlicher CW Jr, Lee TJ (1992) Chem Phys Lett 189: 266
28. Marian CM (1993) Chem Phys Lett 215: 582
29. Fournier R (1993) J Chem Phys 98: 8041
30. Fournier R (1993) J Chem Phys 99: 1801
31. Bauschlicher CW Jr (1994) J Chem Phys 100: 1215
32. Jeung G, Haettel S (1997) Int J Quantum Chem 61: 547
33. Mehner T, Schnöckel H, Almond MJ, Downs AJ (1988) J Chem Soc Chem Commun 117
34. Chenier JHB, Howard JA, Joly HA, Mile B, Timms PL (1990) J Chem Soc Chem Commun 581
35. Mehner T, Köppe R, Schnöckel H (1992) Angew Chem Int Ed Engl 31: 638

36. Williams AP, Van Zee RJ, Weltner W Jr (1996) J Am Chem Soc. 118: 4498
37. Quelch GE, Grev RS, Schaefer HF III (1989) J Chem Soc Chem Commun 1498
38. Tse JS (1990) J Chem Soc Chem Commun 1179
39. Alikhani ME (1997) J Chem Soc Faraday Trans 93: 3305
40. Zhou M, Andrews L (1999) J Chem Phys 111: 4548
41. Bader RFW (1994) Atoms in molecules: a quantum theory Oxford University Press, Oxford
42. Silvi B, Savin A (1994) Nature 371: 683
43. Frisch MJ, Trucks GW, Schlegel HB, Gill PMW, Johnson BG, Robb MA, Cheeseman JR, Keith T, Petersson GA, Montgomery JA, Raghavachari K, Al-Laham MA, Zakrzewski VG, Ortiz JV, Foresman JB, Cioslowski J, Stefanov BB, Nanayakkara A, Challacombe M, Peng CY, Ayala PY, Chen W, Wong MW, Andres JL, Replogle ES, Gomperts R, Martin RL, Fox DJ, Binkley JS, Defrees DJ, Baker J, Stewart JP, Head-Gordon M, Gonzalez C, Pople JA (1995) Gaussian 94, revision D.4. Gaussian, Pittsburgh, Pa
44. Lee C, Yang W, Parr RG (1988) Phys Rev B 37: 785
45. Dolg M, Wedig U, Stoll H, Preuss H (1987) J Chem Phys. 86: 866
46. Andrae D, Haeussermann U, Dolg M, Stoll H, Preuss H (1990) Theor Chim Acta 77: 123
47. Krishnan R, Binkley JS, Seeger R, Pople JA (1980) J Chem Phys 72: 650
48. Clark T, Chandrasekhar J, Spitznagel GW, Schleyer PVR (1983) J Comput Chem 4: 294
49. Frisch MJ, Pople JA, Binkley JS (1984) J Chem Phys 80: 3265
50. Noury S, Krokidis X, Fuster F, Silvi B (1999) Comput Chem 23: 597
51. Konig FB, Bader R, Tang T (1982) J Comput Chem 13: 317
52. Xie Y, Schaefer HF III (1990) J Chem Phys 93: 1196
53. Antes I, Dapprich S, Frenking G, Schwerdtfeger P (1996) Inorg Chem 35: 2089
54. Joubert L, Silvi B, Picard G (2000) Theor Chem Acc 104: 109
55. Cremer D, Kraka E (1984) Angew Chem Int Ed Engl 100: 627
56. Gillespie RJ, Hargittai I (1991) The VSEPR model of molecular geometry. Allyn, Bacon, Boston, Mass
57. Huber KP, Herzberg G (1979) Molecular spectra and molecular structure constants of diatomic molecules. van Nostrand Reinhold, New York